Gravitational radiation from axisymmetric rotational core collapse

Kei Kotake*
Department of Physics, School of Science, University of Tokyo, 7-3-1 Hongo, Bunkyo-ku, Tokyo 113-0033, Japan

Shoichi Yamada
Science & Engineering, Waseda University, 3-4-1 Okubo, Shinjuku, Tokyo, 169-8555, Japan

Katsuhiko Sato
Department of Physics, School of Science, University of Tokyo, 7-3-1 Hongo, Bunkyo-ku, Tokyo 113-0033, Japan
and Research Center for the Early Universe, School of Science, University of Tokyo, 7-3-1 Hongo, Bunkyo-ku, Tokyo 113-0033, Japan
(Received 8 May 2003; published 28 August 2003)

We perform a series of two-dimensional hydrodynamic simulations of the rotational collapse of a supernova core in axisymmetry. We employ a realistic equation of state (EOS) and take into account electron capture and neutrino transport by the so-called leakage scheme. It is an important step to apply the realistic EOS coupled with microphysics to 2D simulations for computing gravitational radiation in rotational core collapse. We use the quadrupole formula to calculate the amplitudes and the waveforms of the gravitational wave assuming Newtonian gravity. With these computations, we extend the conventional category of the gravitational waveforms. Our results show that the peak amplitudes of the gravitational wave are mostly within the sensitivity range of laser interferometers such as TAMA and the first LIGO for a source at a distance of 10 kpc. Furthermore, we find that the amplitudes of the second peaks are within the detection limit of the first LIGO for the source, and first point out the importance of the detection, since it will give us information as to the angular momentum distribution of evolved massive stars.

DOI: 10.1103/PhysRevD.68.044023 PACS number(s): 04.30.Db

I. INTRODUCTION

Asymmetric core collapse and supernovae have been supposed to be one of the most plausible sources of gravitational radiation for long-baseline laser interferometers [GEO600, Laser Interferometric Gravitational Wave Observatory (LIGO), TAMA, VIRGO] [1]. The detection of the gravitational signal is important not only for direct confirmation of general relativity but also for the understanding of supernovae themselves, because the gravitational wave is the only window that enables us to see directly the innermost part of an evolved star, where the angular momentum distribution and the equation of state are unknown.

Observationally, the asymmetric aspects of the dynamics of supernovae are evident because they have been confirmed by many observations of SN 1987A [2–4] and by the kick velocity of pulsars [5]. On the other hand, there is no theoretical consensus on the origin of asymmetry. However, given the facts that the progenitors of collapse-driven supernovae are rapid rotators on the main sequence [6] and that recent theoretical studies suggest a fast rotating core prior to the collapse [7], rotation should play an important role in the origin of the asymmetric motions in core collapse. It is noted that anisotropic neutrino radiation induced by rotation [8] could induce a jetlike explosion [9] as suggested by observations of SN 1987A.

So far there has been some work devoted to studing gravitational radiation in rotational core collapse [10–16] (see [17] for a review). To be rigorous, reliable core collapse simulations should require the implementation of a realistic equation of state (EOS), an adequate treatment of microphysics (electron capture and other weak interactions) and neutrino transport, and a relativistic treatment of gravitation. However, it is difficult to incorporate all of them at the same time. Therefore previous investigations have partially neglected or approximated the above requirements. So far most of the computations have oversimplified the microphysics. In addition, it has been reported that general relativity does not alter the significant features of gravitational radiation compared with those obtained in the Newtonian approximation, such as the range of gravitational wave amplitudes and frequencies [14]. This situation motivates us to employ a realistic EOS and treat the microphysics adequately in the Newtonian gravity. In this paper, we study the waveforms of gravitational radiation in detail by performing improved rotational core collapse simulations and discuss what information can be extracted from the analysis.

We describe the numerical models in the next section. In the third section, we show the main numerical results. A conclusion is given in the last section.

II. MODELS AND NUMERICAL METHODS

A. Initial models

We know little of the angular momentum distributions in the core of evolved massive stars. Although it is supposed that some instabilities grow and transport angular momentum during quasistatic evolutions, which mode prevails on what time scale is not understood very well at present. Therefore, we assume in this study the following two possible rotation laws.

(1) Shell-type rotation:

*Email address: kkotake@utap.phys.s.u-tokyo.ac.jp

TABLE I. The model parameters.

Model	$T/\|W\|_{\rm init}(\%)$	Rotation law	$R_0, X_0, Z_0 \times 10^8$ (cm)	Ω_0 (s^{-1})
SSL	0.25	Shell type	$R_0=1$	2.8
SSS	0.25	Shell type	$R_0=0.1$	45.1
SCL	0.25	Cylinder	$X_0=1,\ Z_0=1$	2.7
SCS	0.25	Cylinder	$X_0=0.1,\ Z_0=1$	31.3
MSL	0.50	Shell type	$R_0=1$	4.0
MSS	0.50	Shell type	$R_0=0.1$	63.4
MCL	0.50	Cylinder	$X_0=1,\ Z_0=1$	3.8
MCS	0.50	Cylinder	$X_0=0.1,\ Z_0=1$	44.4
RSL	1.50	Shell type	$R_0=1$	6.8
RSS	1.50	Shell type	$R_0=0.1$	112
RCL	1.50	Cylinder	$X_0=1,\ Z_0=1$	6.6
RCS	1.50	Cylinder	$X_0=0.1,\ Z_0=1$	76.8

$$\Omega(r)=\Omega_0\times\frac{R_0^2}{r^2+R_0^2}, \tag{1}$$

where $\Omega(r)$ is the angular velocity, r the radius, and Ω_0, R_0 model constants.

(2) Cylindrical rotation:

$$\Omega(X,Z)=\Omega_0\times\frac{X_0^2}{X^2+X_0^2}\cdot\frac{Z_0^4}{Z^4+Z_0^4}, \tag{2}$$

where X and Z denote the distances from the rotational axis and the equatorial plane, and X_0, Z_0 are model constants. The other parameters have the same meanings as above.

Although recent theoretical studies [7] give estimates for the angular velocity prior to collapse, they are one-dimensional models with uncertainties, and not the final answer. Hence we prefer a parametric approach in this paper. We computed 12 models, changing the combination of the total angular momentum, the rotation law, and the degree of differential rotation. The model parameters are presented in Table I. The models are named after this combination, with the first letter S (slow), M (moderate), R (rapid) representing the initial $T/|W|_{\rm init}$, the second letter S (shell-type), C (cylindrical) denoting the rotation law, and the third letter L (long), S (short) indicating the values of R_0 and X_0, which represent the degree of differential rotation. The initial ratio of rotational energy to gravitational energy is designated as $T/|W|_{\rm init}$. We have chosen 0.25%, 0.5%, 1.5% for $T/|W|_{\rm init}$. The rotational progenitor model [18] corresponds to the model MSL (moderate, shell-type rotation, $R_0=1000$ km) in our simulations, and we take this case as the standard model. We have made precollapse models by taking a density and internal energy distribution from the spherically symmetric $15M_\odot$ model by Weaver and Woosley [29] and by adding the angular momentum according to the rotation laws stated above.

B. Hydrodynamics

The numerical method for hydrodynamic computations employed in this paper is based on the ZEUS-2D code [19]. The code is a Eulerian one based on the finite-difference method and employs the artificial viscosity of von Neumann and Richtmyer to capture shocks. The self-gravity is managed by solving the Poisson equation with the incomplete Cholesky decomposition conjugate gradient method. Spherical coordinates are used and one quadrant of the meridian section is covered with $300(r)\times 50(\theta)$ mesh points. The code is checked by standard tests such as the Sod shock-tube problem. We have made several major changes to the base code to include the microphysics. First we added an equation for the electron fraction to treat electron capture, which is solved separately. We approximated electron captures and neutrino transport by the so-called leakage scheme [20–23]. Second, we incorporated a tabulated equation of state based on relativistic mean field theory [24] instead of the ideal gas EOS assumed in the original code. It is noted that the implementation of the recent realistic EOS to 2D simulations is important progress beyond the previous calculations. For a more detailed description of the methods, see Kotake *et al.* [8].

C. Gravitational wave signal

We follow the methods of [10,11] in order to compute the gravitational waveform. We summarize it in the following for convenience. The amplitude of the gravitational wave $h_{\mu\nu}\equiv g_{\mu\nu}-\eta_{\mu\nu}$ can be calculated by the quadrupole formula as follows:

$$h_{ij}^{\rm TT}(R)=\frac{2G}{c^4}\frac{1}{R}\frac{d^2}{dt^2}I_{ij}^{TT}\left(t-\frac{R}{c}\right), \tag{3}$$

where i,j run from 1 to 3, t is the time, R is the distance from the source to the observer, the superscript "TT" means to take the transverse traceless part, and I_{ij} is the reduced quadrupole defined as

$$I_{ij}=\int\rho(x)\left(x_ix_j-\frac{1}{3}x^2\delta_{ij}\right)d^3x. \tag{4}$$

The second time derivative of the reduced quadrupole formula, which is difficult to treat numerically, can be replaced

by the spatial derivative using the equations of motion. In the case of axisymmetric collapse, the transverse traceless gravitational field is shown to have one independent component $h^{\rm TT}_{\theta\theta}$, and it is dependent solely on $A^{\rm E2}_{20}$. Then one derives for the component of $h^{\rm TT}$ the following formula:

$$h^{\rm TT}_{\theta\theta}=\frac{1}{8}\left(\frac{15}{\pi}\right)^{1/2}\sin^2\theta\frac{A^{\rm E2}_{20}}{R}, \tag{5}$$

where θ is the polar angle and $A^{\rm E2}_{20}$ is defined as

$$A^{\rm E2}_{20}=\frac{G}{c^4}\frac{32\pi^{3/2}}{\sqrt{15\pi}}\int_0^1\int_0^\infty r^2\,dr d\mu\,\rho[v_r^2(3\mu^2-1)+v_\theta^2(2 -3\mu^2)-v_\phi^2-6v_rv_\theta\mu\sqrt{1-\mu^2}-r\partial_r\Phi(3\mu^2-1) +3\partial_\theta\Phi\mu\sqrt{1-\mu^2}], \tag{6}$$

where $\partial_r=\partial/\partial r$, $\partial_\theta=\partial/\partial\theta$, $\mu=\cos\theta$, and Φ is the gravitational potential. Since the gravitational wave radiates most in the equatorial plane, the observer is assumed to be located in the plane in the following discussions. In addition, the source is assumed to be located at a distance of $R=10$ kpc.

III. NUMERICAL RESULTS

A. The properties of the waveform

We first show the general properties of the waveform with collapse dynamics. We choose the model MSL (standard) as a representative model. For later convenience, the values of several important quantities are summarized in Table II. The time evolution of the amplitude of the gravitational wave and the central density near core bounce are shown in Fig. 1. As the inner core shrinks, the central density increases, and a core bounce occurs when the central density reaches its peak of 2.65×10^{14} g cm^{-3} at $t_{\rm b}\cong243$ ms. At this time, the absolute value of the amplitude becomes maximum. After the core bounce, the core slightly reexpands and oscillates around its equilibrium value. As a result, the gravitational wave shows several small bursts and begins to decay. These gross properties are common to all other models. However, there exist some important differences when we compare them in more detail. We will discuss the differences in the following.

TABLE II. Summary of important quantities for all models. $t_{\rm b}$ is the time of bounce, $\rho_{\rm maxb}$ is the maximum density at bounce, $M_{\rm ic\,b}$ is the mass of the inner core at bounce, $T/|W|_{\rm final}$ is the final ratio of rotational energy to gravitational energy of the core, Δt is the duration time full width at half maximum of the first burst, and $|h^{\rm TT}|_{\rm max}$ is the maximum amplitude of the first burst. Note that we speak of the inner core, where the matter falls subsonically, which corresponds to the unshocked region after core bounce.

Model	$t_{\rm b}$ (ms)	$\rho_{\rm maxb}$ (10^{14} g cm^{-3})	$M_{\rm ic\,b}$ ($M_\odot$)	$T/\lvert W\rvert_{\rm final}$ (%)	Δt (ms)	$\lvert h^{\rm TT}\rvert_{\rm max}$ (10^{-20})
SSL	227.4	2.95	0.74	4.87	0.58	1.03
SSS	227.3	2.80	0.75	5.66	0.54	1.49
SCL	241.2	2.87	0.75	5.09	0.46	0.93
SCS	230.7	2.84	0.73	6.46	0.56	2.00
MSL	242.7	2.65	0.75	8.44	0.72	1.58
MSS	242.2	2.15	0.87	9.05	0.57	2.03
MCL	241.9	2.85	0.76	8.38	0.70	1.53
MCS	245.4	1.45	0.91	9.94	0.51	2.87
RSL	338.7	1.21	0.94	14.6	2.89	0.48
RSS	328.6	0.53	0.96	13.3	2.80	0.78
RCL	338.4	1.36	0.95	14.5	4.47	0.42
RCS	326.7	0.18	1.11	12.3	1.91	1.41

In Fig. 2, the time evolution of the amplitude of the gravitational wave and the central density near core bounce for the model MCS are given. For the model, it is noted that the initial rotation law is cylindrical with strong differential rotation. By comparing the left panel of Fig. 1 to that of Fig. 2, the oscillation period of the inner core for the model MCS is clearly seen to be longer than that for the model MSL. In other words, pronounced peaks can be seen distinctively in this case. This is because the central density becomes smaller after the distinct bursts (compare the right panel of Fig. 1 to that of Fig. 2). This effect increases with the initial angular momentum (compare the left panel of Fig. 2 to that of Fig. 3). It is also found that the signs of the values of the second peaks are negative for model MCS, but positive for model MSL (compare the left panels of Figs. 2 and 1). Note that by

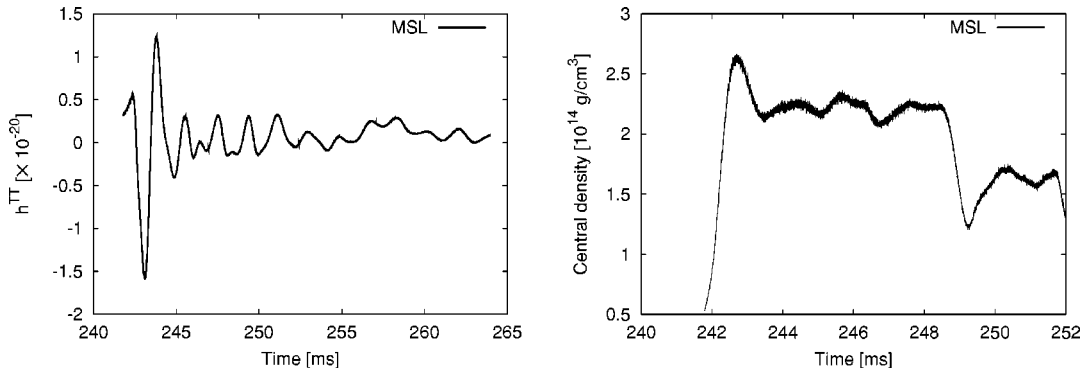

FIG. 1. Time evolution of the amplitude of the gravitational wave (left panel) and central density near core bounce (right panel) for the model MSL.

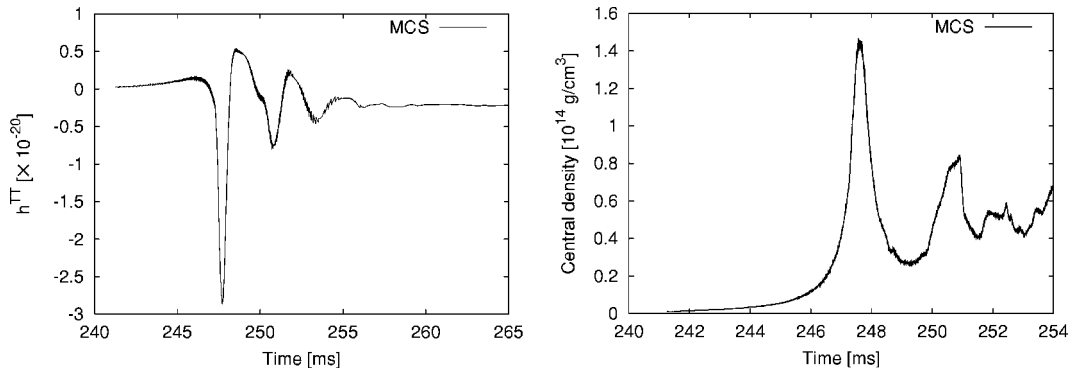

FIG. 2. Same as Fig. 1 but for the model MCS.

the ''second peak'' we mean that where the absolute amplitude is second largest. The above characteristics are common to models for strongly differential rotation with a cylindrical rotation law (see Table III). A specific feature in the waveform is found for models RSL and RSS in which there exists a small peak or shoulder before the peak burst (see the right panel of Fig. 3).

Next we compare our results for the waveforms with those by Zwerger and Müller [12], who categorized the shapes of waveforms into three district classes. They used a polytropic EOS to express the pressure from the degenerate leptons as $P \propto \rho^{\gamma}$. They reduced the adiabatic index γ from 1.325 to 1.28 below the nuclear density regime in order to approximate the related microphysics and neutrino transport. They assumed the cylindrical rotation law for all the models and varied both the degree of differential rotation and the initial angular momentum. Our models except for the strongly differential rotation with the cylindrical rotation law correspond to the so-called type I in their nomenclature. On the other hand, our models for strongly differential rotation with a cylindrical (not shell-type) rotation law correspond to their type II. It should be noted that type II signals were limited, occuring only for rapid, strongly differential rotation with a cylindrical rotation law in their models. Furthermore, in this study, we find that type II does not occur for models with a shell-type rotation law, regardless of the degree of differential rotation and the initial rotation rate; on the other hand, it does occur regardless of the initial rotation rate in the case of strong differential rotation with a cylindrical rotation law. Finally, type III occurred only when the core collapses very rapidly ($\gamma = 1.28$) in their calculations. There are no models that correspond to that type in our calculations. This is because our realistic EOS is not as soft in the corresponding density regime.

B. Maximum amplitude and second peak

We first discuss the relation between the maximum amplitude of the gravitational wave and the initial $T/|W|$. The maximum values and the related quantities are given in Tables I and II. From Fig. 4, it is found that the amplitude is largest for a moderate initial rotation rate (i.e., $T/|W|_{\rm init} = 0.5\%$) when one fixes the initial rotation law and the degree of differential rotation. This is understood as follows. The amplitude of a gravitational wave is roughly proportional to the inverse square of the typical dynamical scale $t_{\rm dyn}$ [e.g., Eq. (3)]. Since $t_{\rm dyn}$ is proportional to the inverse root of the central density ρ, the amplitude is proportional to the density. As a result, the amplitude becomes smaller as the initial rotation rates become larger, because the density decreases for a large initial rotation rate (see Table II and Fig. 5). On the other hand, the amplitude is proportional to the value of the quadrupole moment, which becomes large in turn as the total angular momentum increases. This is because the stronger centrifugal forces not only make the mass of the inner core larger (see Table II), but also deform the inner core. The amplitude is determined by the competition between these factors. As a result, the amplitude becomes extreme for moderate initial rotation rates in our calculation.

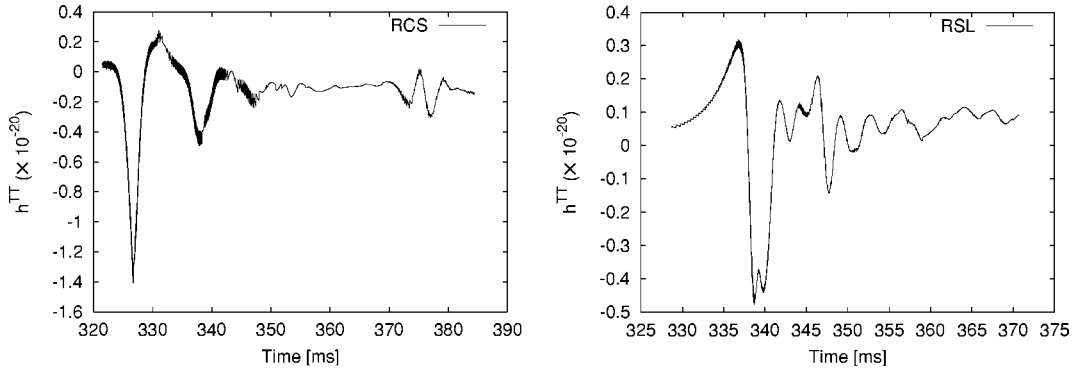

FIG. 3. Waveforms for models RCS (left panel) and RSL (right panel). In the left panel, very distinct peaks are seen. In the right panel, a small peak and shoulder after the first burst can be seen.

TABLE III. Some characteristic quantities for the waveform analysis. The names of the models whose initial rotation law is cylindrical with strong differential rotation are written in bold letters. $T^{\rm I}_{\rm osc}$ and $T^{\rm II}_{\rm osc}$ are the first and second oscillation periods of the inner core, respectively. $h^{\rm TT}_{\rm second}$ is the amplitude of the gravitational wave at the second peak.

Model	$T^{\rm I}_{\rm osc}$ (ms)	$T^{\rm II}_{\rm osc}$ (ms)	$h^{\rm TT}_{\rm second}$ (10^{-20})
SSL	1.6	2.4	0.82
SSS	1.5	2.2	0.94
SCL	1.6	2.3	0.75
SCS	1.8	2.6	−0.57
MSL	1.8	1.2	1.23
MSS	2.2	2.4	0.98
MCL	1.7	1.1	1.20
MCS	3.1	2.6	−0.79
RSL	1.0	3.1	0.32
RSS	1.0	7.8	0.20
RCL	9.0	2.9	0.25
RCS	10.7	8.6	−0.49

Next we discuss the values of the maximum amplitude, comparing our results with those by other groups. The values of maximum amplitude for all our models are in the range $5\times10^{-21}\leqslant h^{\rm TT}\leqslant 3\times10^{-20}$, which is almost the same as the results of Zwerger and Müller [12] and Mönchmeyer *et al.* [10]. On the other hand, the values obtained with the standard models by Yamada and Sato [11] are about an order of magnitude lower. This is understood as follows. Yamada and Sato [11] employed a parametric EOS by which the effects of microphysical and transport processes were assumed to be expressed. Since they found that the maximum amplitude is most sensitive to the adiabatic index at subnuclear density by their parametric surveys, we pay attention to this. A comparison of the effective adiabatic index between our EOS and their EOS is shown in Fig. 6. Compared to their EOS, our realistic EOS is rather soft in the subnuclear density regime. In this regime, our realistic EOS can express the softening of the EOS caused by the effect that the nuclear interactions become attractive. Due to this effect, the inner core can become more compact at core bounce, which results in a larger maximum amplitude. It is naturally suggested that we may get information about the subnuclear matter if we can detect a gravitational wave from a rotationally collapsing core. We hope this can be realized in the near future, since the maximum amplitudes for our models are mostly within the detection limits for TAMA and first LIGO, which are now in operation, if a source is located at a distance of 10 kpc (see Fig. 7).

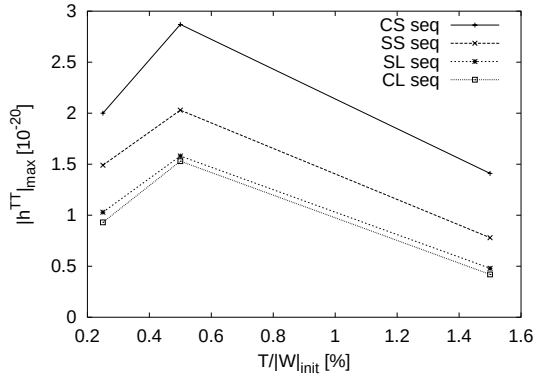

FIG. 4. Relation between $T/|W|_{\rm init}$ and the peak amplitude $|h^{\rm TT}|_{\rm max}$ for all the models. CS, SS, SL, and CL seq in the figure represent the model sequences, whose names are taken from the second and third letters in Table I. Note that the second and third letters mean the rotation law and the degree of differential rotation, respectively.

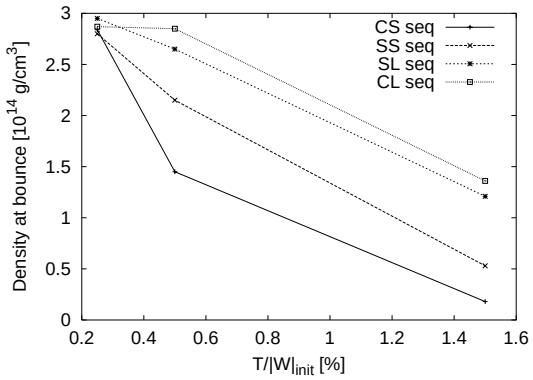

FIG. 5. Relation between $T/|W|_{\rm init}$ and the central density at core bounce (10^{14} g cm^{-3}) for all the models. The labels are the same as in Fig. 4. It is found that the central density at the core bounce becomes smaller as the initial angular momentum becomes larger.

As pointed out earlier, we find that the signs of the values of the second peaks are negative for models with strongly differential rotation with a cylindrical rotation law and positive for the others (see Table III). The absolute amplitudes of the second peak are also presented in Fig. 7. As shown, they are within the detection limit of first LIGO for a source at a distance of 10 kpc. In addition, it seems quite possible for detectors in the next generation, such as advanced LIGO and LCGT, to detect the difference. Therefore if we can find a difference in the signs of the second peaks by observations of gravitational waves, we will obtain information about the

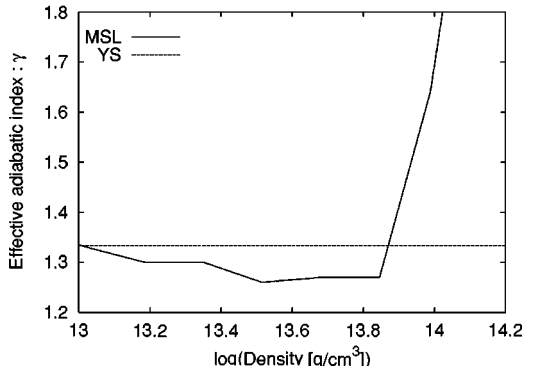

FIG. 6. Relation between the density and the effective adiabatic index γ at subnuclear density. MSL represents the relation for our standard model. On the other hand, the index employed in the study of Yamada and Sato [11] is represented as YS.

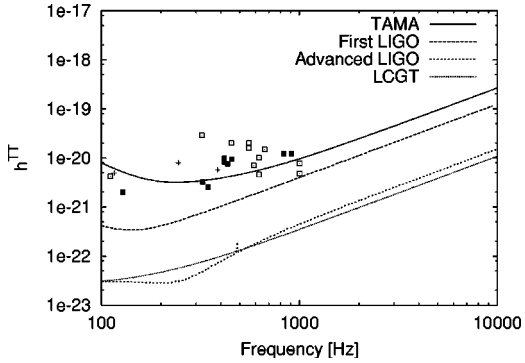

FIG. 7. Detection limits of TAMA [25], first LIGO [26], advanced LIGO [27], and Large-scale Cryogenic Gravitational wave Telescope (LCGT) [28], with the expected amplitudes from numerical simulations. The open squares represent the maximum amplitudes for all the models. On the other hand, the pluses and the closed squares represent the amplitudes of the second peaks for models with strong differential rotation with a cylindrical rotation law and for the other models, respectively. We estimate the characteristic frequencies using the inverse of the duration period of the corresponding peak. Note that the source is assumed to be located at a distance of 10 kpc.

angular momentum distribution of evolved massive stars. Since there is no way except for the detection of a gravitational wave to obtain the information, it is of great importance to detect the second peaks in the future.

C. Secular instability

In some models (models RSL and RCS) with a large initial rotation rate, the final rotation rate exceeded the critical value (see Table II) where MacLaurin spheroids become secularly unstable against triaxial perturbations ($T/|W|>T/|W|_{\rm seq}=13.75\%$). Rampp *et al.* [13] reported that no considerable enhancement of gravitational radiation due to the growth of secular instabilities was found within a time scale of several tens of milliseconds after core bounce. Since our calculations are within this time scale, the axial symmetry assumed in this work may be justified.

IV. CONCLUSION

We have done a series of two-dimensional hydrodynamic simulations of the rotational collapse of a supernova core and calculated gravitational waveforms using the quadrupole formula. We employed a realistic EOS and took into account electron capture and neutrino transport in an approximate method. We found the following.

(1) The peak amplitudes of the gravitational wave obtained in this study are mostly within the detection limits of the detectors of TAMA and first LIGO, which are now in operation, if a source is located at a distance of 10 kpc. In addition, the peak amplitude becomes extreme for models whose initial rotation rate is moderate.

(2) The waveforms are categorized into the criteria by Zwerger and Müller [12]. In addition, we further find that type II does not occur for models with a shell-type rotation law; on the other hand, it does occur regardless of the initial rotation rate in the case of strong differential rotation with a cylindrical rotation law. Type III does not occur if a realistic EOS is employed.

(3) In the subnuclear density regime, our realistic EOS can express the softening of the EOS caused by the nuclear interactions becoming attractive. Therefore the inner core can shrink and become more compact at core bounce than in [11], in which the EOS is expressed in a parametric manner. Subsequently, this results in a larger maximum amplitude. It follows that we may get information about the subnuclear matter if we can detect the gravitational waves from rotationally collapsing cores.

(4) The signs of the values of the second peaks are negative for models with strong differential rotation with a cylindrical rotation law; on the contrary, they are positive for the other models. The absolute amplitudes of the second peaks are within the detection limit of first LIGO. Therefore, if we can detect the signs of the second peaks, it will give us information as to the angular momentum distribution of massive evolved stars when a supernova occurs at our galactic center.

As stated earlier, the detection of gravitational waves is likely for models whose initial rotation rate is moderate. According to the study of rotational core collapse by Kotake *et al.* [8], anisotropic neutrino radiation is easily induced by such a rotation rate. Noting that anisotropic neutrino radiation can induce a globally asymmetric explosion [9], the detection of gravitational waves will be a good tool to help understand the explosion mechanism itself.

ACKNOWLEDGMENTS

We are grateful to K. Numata and M. Ando for helpful discussions. K.K. would like thank M. Oguri and M. Shimizu for supporting computer environments. The numerical calculations were partially done on the supercomputers at RIKEN and KEK (KEK Supercomputer Projects No. 02-87 and No. 03-92). This work was partially supported by Grants-in-Aid for Scientific Research from the Ministry of Education, Science and Culture of Japan through Grants No. S 14102004, No. 14079202, and No. 14740166.

[1] C. Cutler and K.S. Thorne, in Proceedings of GR16, Durban, South Africa, 2001 (to be published).
[2] M. Cropper *et al.*, Mon. Not. R. Astron. Soc. **231**, 695 (1988).
[3] C. Papaliolis *et al.*, Nature (London) **338**, 13 (1989).
[4] L. Wang *et al.*, Astrophys. J. **579**, 671 (2002).
[5] A. Lyne and D.R. Lorimer, Nature (London) **369**, 127 (1994).
[6] J.L. Tassoul, *Theory of Rotating Stars* (Princeton University Press, Princeton, NJ, 1978).
[7] A. Heger, N. Langer, and S.E. Woosley, Astrophys. J. **528**, 368 (2000).

[8] K. Kotake, S. Yamada, and K. Sato, Astrophys. J. (to be published).
[9] T.M. Shimizu, T. Ebisuzaki, K. Sato, and S. Yamada, Astrophys. J. **552**, 756 (2001).
[10] R. Mönchmeyer, G. Schäfer, E. Müller, and R.E. Kates, Astron. Astrophys. **246**, 417 (1991).
[11] S. Yamada and K. Sato, Astrophys. J. **450**, 245 (1995).
[12] T. Zwerger and E. Müller, Astron. Astrophys. **320**, 209 (1997).
[13] M. Rampp, E. Müller, and M. Ruffert, Astron. Astrophys. **332**, 969R (1998).
[14] H. Dimmelmeier, J.A. Font, and E. Müller, Astron. Astrophys. **393**, 523D (2002).
[15] C.L. Fryer, D.E. Holz, and S.A. Hughes, Astrophys. J. **565**, 430 (2002).
[16] M. Shibata, Phys. Rev. D **67**, 024033 (2003).
[17] K.S. New, Living Rev. Relativ. (to be published), gr-qc/0206041.
[18] C.L. Fryer and A. Heger, Astrophys. J. **541**, 1033 (2000).
[19] J.M. Stone and M.L. Norman, Astrophys. J., Suppl. Ser. **80**, 753 (1992).
[20] R.I. Epstein and C.J. Pethick, Astrophys. J. **243**, 1003 (1981).
[21] S.A. Bludman, I. Lichtenstadt, and G. Hayden, Astrophys. J. **261**, 661 (1982).
[22] K.A. van Riper and J.M. Lattimer, Astrophys. J. **249**, 270 (1981).
[23] K.A. van Riper, Astrophys. J. **257**, 793 (1982).
[24] H. Shen, H. Toki, K. Oyamatsu, and K. Sumiyoshi, Nucl. Phys. **A637**, 43 (1998).
[25] TAMA Collaboration, M. Ando, Class. Quantum Grav. **19**, 1409 (2002).
[26] K.S. Thorne, in *Proceedings of the Snowmass 95 Summer Study on Particle and Nuclear Astrophysics and Cosmology* (World Scientific, Singapore, 1995), pp. 398–425.
[27] A. Weinstein, Class. Quantum Grav. **19**, 1575 (2002).
[28] LCGT Collaboration, K. Kuroda *et al.*, Int. J. Mod. Phys. D **8**, 557 (1999).
[29] T.A. Weaver and S.E. Woosley (private communication).